Final Technical Report for DARPA contract, HR0011-10-C-0073, “AWARE Wide Field View”

Performing Organization:
Duke University
2200 W. Main St., Ste. 710
Durham, NC 27705

Contracting Agency:
Defense Advanced Research Projects Agency
CMO
3701 N. Fairfax Drive
Arlington, VA 22203-1714

AWARE Wide Field of View

DARPA MTO AWARE Program
Contract Number HR0011-10-C-0073

Final Report

Submitted by David J. Brady, dbrady@duke.edu,
919 660 5394

Summary

The DARPA AWARE Wide Field of View program successfully demonstrated that a common microcamera platform can be used to quickly and effectively provision wide field of view high resolution cameras with pixel counts between 0.25 and 10 gigapixels. The array camera architecture uniquely allows high depth of field and high dynamic range imaging using independent parallel control of the microcamera array. Moving forward, the array camera approach will be applied to diverse applications in visible and infrared imaging.

AWARE produced four gigapixel camera systems: the AWARE 2 with a 40 μrad instantaneous-field-of-view (IFOV) and 0.3 to 1 gigapixel, the AWARE 10 with 25 μrad IFOV and 1 to 4 gigapixels, the AWARE 40 with 12 μrad IFOV and 3 gigapixels, and the MOAC with 17 μrad and 8 to 11 gigapixels. The prototypes of the AWARE 2 and 40 cameras are shown below. The project has realized DARPA's goal of achieving a scalable, modular, and economic architecture including a design methodology and completed prototypes. Furthermore, the project has already demonstrated surveillance capability far superior to existing shipboard naval surveillance systems by reliable identification of potential threat watercraft as small as 7 m at a distance of 6 km over a 100° field-of-view (FOV) with the AWARE 10 camera. While this initial demonstration showed the great potential applications of the DARPA-sponsored technology to provide the resolution of a telescope over a wide-field, further demonstrations and adaptations would speed the adoption and ease the transition of the technology to the armed services. The four architectures that have been constructed are adaptable to urgent and unsatisfied applications including wide-field high-resolution aerial reconnaissance, space situational awareness, terrestrial perimeter surveillance, as well as the naval threat identification applications already explored.

AWARE 2 folded camera, 40 μrad IFOV, 50° by 30° FOV, fits in a commercial airline carry-on bag.

AWARE 40 camera
12 μrad IFOV, 30° FOV

Requirements and Specifications

The original program considered construction of a 50 gigapixel camera. Design analysis and optical testing confirmed the feasibility of such a camera, but budget constraints limited as built systems to 10 gigapixels. Specifically, an array of 3 AWARE 40 cameras was shown to be capable of meeting the demonstration specifications listed below. The performance of this system is reported in Patrick Llull, Lauren Bange, Zachary Phillips, Kyle Davis, Daniel L. Marks, and David J. Brady, "Characterization of the AWARE 40 wide-field-of-view visible imager," Optica **2**, 1086-1089 (2015)

MOSAIC Phase II demonstration	
Integrated optical and opto-electronic prototype volume	0.25 cubic meter
Prototype mass	90 kg
Field of view (FOV)	100 by 60 degree
Instantaneous field of view (ifov)	16.6 microradian cone angle
Image size	10 gigapixel
Image type	RGB color
Operating modes	Full frame snapshot and live streaming interface

Image quality	Comparable to 600 mm Canon SLR baseline
Motion and turbulence artifacts	Component level demonstration
Frame rate	6 Hz
Frame buffer	>30
Image formation latency	<1 second

The AWARE program was pursued in two phases, in the first phase a gigapixel camera was constructed and tested with results reported in Brady, D. J., et al. (2012). "Multiscale gigapixel photography." Nature 486(7403): 386-389.

The second phase used next generation glass optics and an improved processor architecture.

Project tasks included system design, optical design, electronic system design and prototype construction and testing.

Results for these tasks were reported in peer reviewed publications.

Publications considering limits of AWARE system performance include

Brady, D. J., et al. (2013). Petapixel Photography and the Limits of Camera Information Capacity. Computational Imaging Xi. C. A. Bouman, I. Pollak and P. J. Wolfe. 8657.

Marks, D. L. and D. J. Brady (2011). "Close-up imaging using microcamera arrays for focal plane synthesis." Optical Engineering 50(3).

Marks, D. L. and D. J. Brady (2013). "Wide field astronomical multiscale cameras." Astronomical Journal 145(5).

Publications reporting results from camera systems tests include

Brady, D. J., et al. (2012). "Multiscale gigapixel photography." Nature 486(7403): 386-389.

Llull, P., et al. (2015). "Characterization of the AWARE 40 wide-field-of-view visible imager." Optica 2(12): 1086-1089.

Marks, D. L., et al. (2014). "Characterization of the AWARE 10 two-gigapixel wide-field-of-view visible imager." Applied Optics 53(13): C54-C63.

Publications describing the image processing pipeline include

Golish, D. R., et al. (2012). "Development of a scalable image formation pipeline for multiscale gigapixel photography." Optics Express 20(20): 22048-22062.

Iliopoulos, A. S., et al. (2013). Big Snapshot Stitching with Scarce Overlap, 2013 IEEE Conference on High Performance Extreme Computing

Marks, D. L., et al. (2015). "Feedback stitching for gigapixel video." Journal of Electronic Imaging 24(6).

Nakamura, T., et al. (2013). "Autofocus for a multiscale gigapixel camera." Applied Optics 52(33): 8146-8153.

Publications describing optical system design and performance include

Marks, D. L., et al. (2011). "Microcamera aperture scale in monocentric gigapixel cameras." Applied Optics 50(30): 5824-5833.

Tremblay, E. J., et al. (2012). "Design and scaling of monocentric multiscale imagers." Applied Optics 51(20): 4691-4702.

Zheng, N., et al. (2012). "Computer experiment and global optimization of layered monocentric lens systems." Optik 123(14): 1249-1259.

Publications describing optomechanical design and testing include

Marks, D. L., et al. (2012). "Engineering a gigapixel monocentric multiscale camera." Optical Engineering 51(8).

Kittle, D. S., et al. (2013). Automated calibration and optical testing of the AWARE-2 gigapixel multiscale camera. Digital Photography Ix. N. Sampat and S. Battiato. 8660.

Kittle, D. S., et al. (2013). "A testbed for wide-field, high-resolution, gigapixel-class cameras." Review of Scientific Instruments 84(5).

Son, H. S., et al. (2013). "Optomechanical design of multiscale gigapixel digital camera." Applied Optics 52(8): 1541-1549.

Son, H. S., et al. (2013). "Oversampled triangulation of AWARE-10 monocentric ball lens using an auto-stigmatic microscope." Optics Express 21(19): 22206-22214.

Son, H. S., et al. (2011). "Design of a spherical focal surface using close-packed relay optics." Optics Express 19(17): 16132-16138.

Son, H. S., et al. (2013). "Design of a spherical focal surface using close-packed relay optics: erratum." Optics Express 21(22): 27284-27285.

Son, H. S., et al. (2013). Alignment and assembly strategies for AWARE-10 gigapixel-scale cameras. Optomechanical Engineering 2013. A. E. Hatheway. 8836.

Youn, S. H., et al. (2013). Efficient testing methodologies for microcameras in a gigapixel imaging system. Optical Measurement Systems for Industrial Inspection Viii. P. H. Lehmann, W. Osten and A. Albertazzi. 8788.

Youn, S. H., et al. (2014). "Optical performance test and validation of microcameras in multiscale, gigapixel imagers." Optics Express 22(3): 3712-3723.

Technology transition was also a critical component of the AWARE program. DARPA supported a follow project with Applied Quantum Technologies, in Durham, NC to support continued operation of the AWARE cameras and development of next generation systems. As part of this project, additional tests on at the Naval Research Laboratory testing sight on the Chesapeake Bay were conducted in collaboration with J. M. Nichols, C. C. Olson, K. P. Judd, K. Novak of NRL. The results of this study will be submitted in a future peer reviewed publication. A draft version of the study is included below.

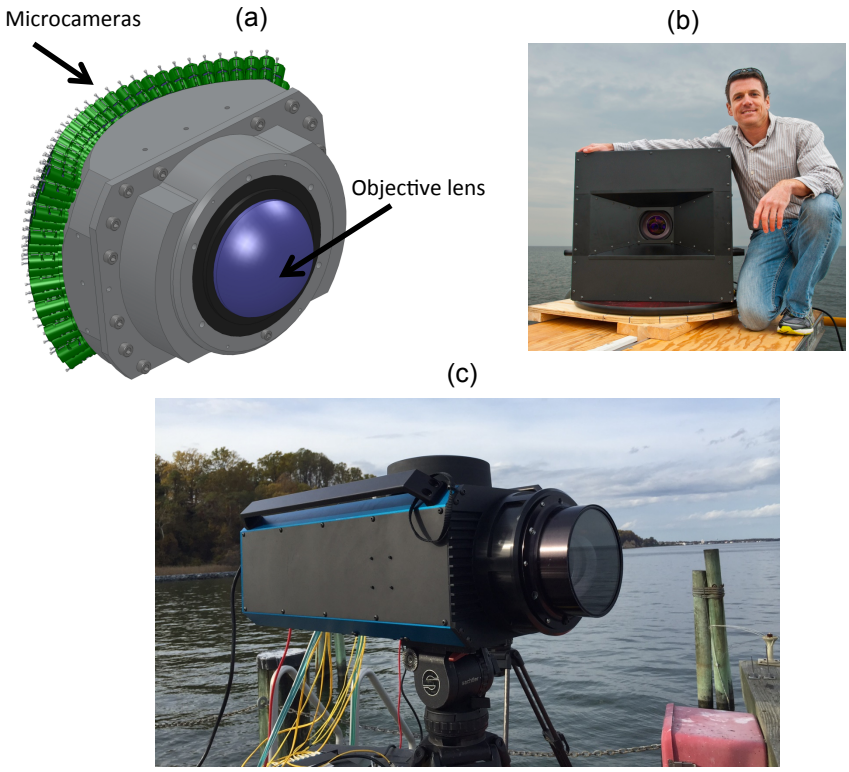

FIG. 1. (a) Basic AWARE camera architecture whereby a single, spherical objective lens distributes the incident scene across an array of visible micro-cameras. (b) The original AWARE camera system occupying a volume $> 0.15\ m^3$ and consuming $> 1kW$ of power. (c) The new AWARE camera measuring $0.305m \times 0.228m \times 0.762m$ ($0.053\ m^3$), weighing 19kg and consuming roughly 100 Watts of power

I. BACKGROUND

In a prior work, [1], we documented the design and performance of a new camera architecture developed as part of the DARPA Advanced Wide FOV Architectures for Image Reconstruction and Exploitation program (referred to herein as AWARE). The goal of AWARE is to simultaneously provide both wide field-of-view (FOV) imaging capability and the resolution required to detect and identify distant targets. This was accomplished by leveraging the power of a large number of small, cheap focal plane arrays to produce a single, high-resolution image over a wide FOV. Specifically, the previous system afforded the user a 100° by 60° field-of-view with an instantaneous FOV of 25μrad; a resolution that meets many of the Navy's requirements for identifying targets at range. These twin objectives were met by distributing light from a single aperture over a large number of micro-cameras using a spherical objective lens as shown in Figure (1a). The resulting architecture has the advantage of being highly modular and easily scalable to larger FOVs as one can simply populate the camera housing with additional micro-cameras as dictated by the application.

While the system simultaneously addresses multiple (competing) imaging requirements, the challenge lies in minimizing the physical footprint of the system. The previous architecture occupied a volume of $> 0.15\ m^3$, and consumed $> 1\ kW$ of power; this system is shown in Figure (1b). Over the last two years we have therefore worked to maintain or improve the system optical performance (e.g., target identification), while significantly reducing the system size, weight and power. The end result is shown in Figure (1c) and achieves both of these aims.

In what follows we document and compare this new generation of camera with the previous version. We then repeat the maritime target identification experiment performed in reference [1] and provide a comparison of the resulting range performance curves. The results obtained for the new, smaller system show significant improvement in range performance over the previous incarnation.

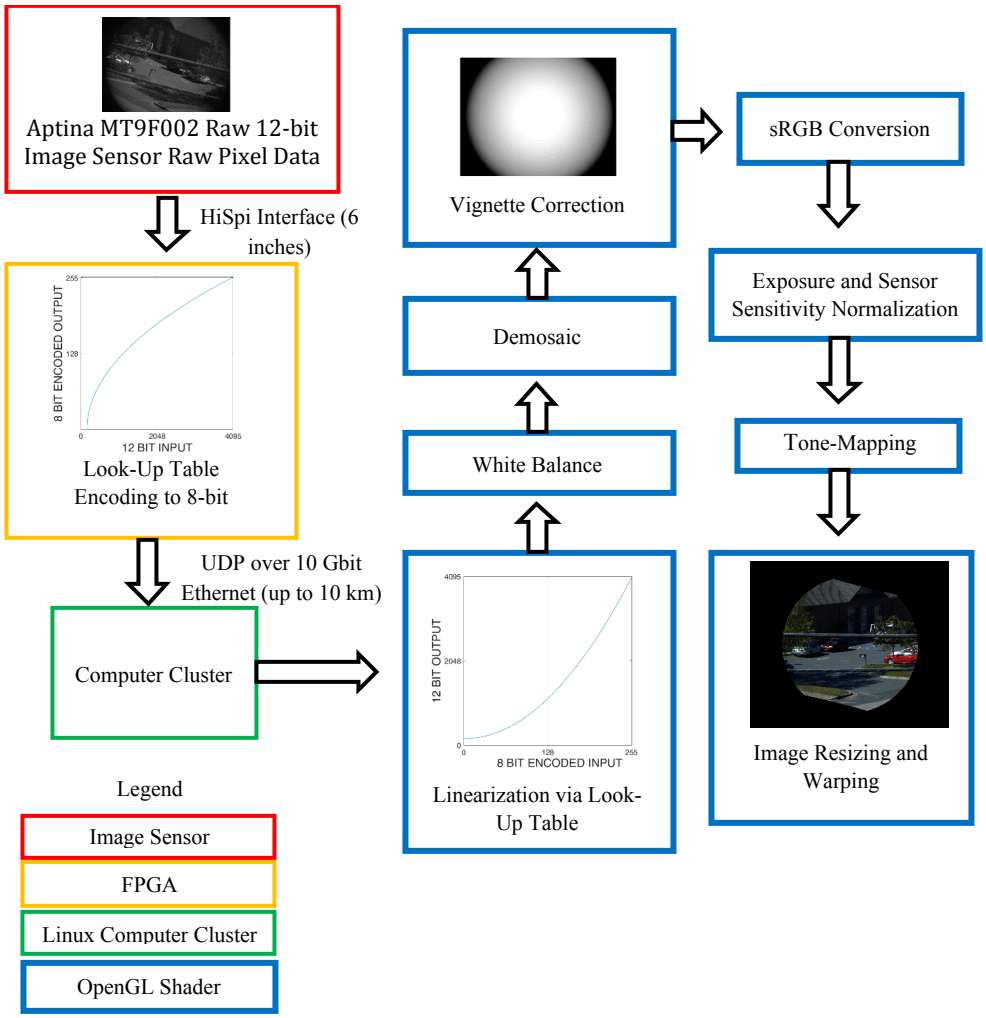

FIG. 2. Image processing pipeline for a single micro-camera

II. IMPROVED CAMERA ARCHITECTURE

In addition to minimizing system size, weight, and power (SWaP), two major areas were identified for improvement over the previous AWARE camera: micro-camera focus and optimization of the image processing pipeline. Regarding the former, significant improvements were obtained by adding hardware-based auto-focus to this system. Specifically, auto-focus was performed by adding a contrast detection algorithm onto the field-programmable gate arrays (FPGA) that managed the data capture and controlled the focus positioner. This allowed for automated focusing of each individual micro-camera which was faster and more reliable than the manual focusing done in the earlier experiment documented in [1].

Additional improvements were made to both the image processing pipeline as well as the data routing architecture required to move the large volume of data reliably and efficiently from camera to computer. Both of these areas are discussed next.

A. Image Processing Improvements

The overall data processing pipeline for the new system is shown schematically in Figure (2). By improving the image processing pipeline, the detection task was made easier by providing higher fidelity images with better calibration. The image processing pipeline was optimized by mapping the 12-bit sensor data non-linearly onto the 8-bit data flow that the FPGA required for data transmission. A look-up table (LUT) was generated with a power

law of 0.5,

$$P_{comp} = P_{raw}^{1/2} \tag{1}$$

Where P_{raw} is the linear 12-bit sensor pixel data and P_{comp} is the compressed pixel data which is then quantized at 8-bits. The end result of this was to match the quantization spacing of the measured data with the Poisson noise of the measured data (which has a similar square root dependence). The original AWARE system performed this 12 to 8 bit conversion by dropping the last 4 bits of the image sensor data. This 8-bit data was then sent packetized and transmitted by the FPGA to the computer cluster where it was stored in local memory and then either written to disk, sent to the rendering system if needed, or temporarily cached.

The image rendering task of assembling one zoomable image from an array of image sensors followed the same geometrical mapping developed in [1]. Changes in the rendering pipeline focused mostly on the radiometric processing of the sensor data. After linearizing the sensor data based on the LUT applied at the FPGA, a white balance was applied by scaling the sensor data that corresponded to the Bayer color filter channels (one red, two green, and one blue) on the sensor. Each image sensor had its white balance scaled differently based on a flat field calibration measurement done by placing a diffuser in front of the entire camera during calibration. Demosaicing was performed efficiently in the OpenGL shader by using kernels similar to the approach of Malvar *et al.* [2].

Vignetting correction was accomplished by performing a pixel-by-pixel scaling of the demosaiced imagery based on a flat field measurement captured during calibration. The parameters of the vignetting included the center point of the radial map, and three 10th order polynomial fits describing the radial roll-off for each color channel. After this vignetting correction, a 3x3 matrix multiplication converts the sensor RGB colors to the standard sRGB to allow spectrally consistent colors on monitors for viewing. Finally, the images from each sensor are corrected based on the exposure time used and the calibrated sensitivity of each image sensor, again based on the flat field calibration, to allow viewing of imagery from different sensors on the same display. A global tone-mapping is then controlled at the rendering system by adjusting brightness and contrast to optimize the display of imagery. The image resizing and warping is done to map the correct data from the sensor array to render the view of interest to the user. A joystick provided pan, zoom, and tilt navigation through the field-of-view with buttons for pausing and advancing backwards and forwards in time.

B. Improvements in Data Routing Architecture

One of the chief problems encountered when developing systems with very large formats is physically moving the data from camera to display. In this section we discuss the changes in the data routing architecture and operating system to improve performance. These changes including a new data routing paradigm, advanced image caching architecture, and better prediction algorithms for real-time data access. These changes were driven by the need to make a more compelling user interface through decreased latency, improved frame rate and a more responsive user feedback.

For the AWARE camera discussed in this paper, this architecture is able to provide multiple interactive user interfaces to a single camera with image updates approaching 5.6 frames per second with less than a second latency from a real-world event. This is significantly more responsive that our previous implementation while maintaining the flexibility to scale the system to an arbitrary number of sensors without significant degradation in performance. Figure (3) outlines the new system architecture:

The original architecture implemented a state machine for rendering individual frames. For each frame, the rendering system would calculate the scale and a region of interest required by each camera to render the scene to the display. This list of image requests would then get transferred to the embedded FPGAs, on the system which would resize and crop the raw image data before sending a final image of the appropriate resolution and scale. In the interim, the user would be able to interact with the current frame until the requested one arrives. This approach minimizes the number of pixels transmitted to the rendering system, but its sequential nature limited the screen update rate to two frames per second and leads to significant lag before an event would appear on screen. In addition, the embedded hardware had very limited storage capacity, so this precluded storage of video sequences more that about 30 frames in size.

The current camera architecture was designed for real-time video broadcast applications and uses a parallel acquisition and rendering architecture to minimize latency and provide full-resolution video capture support. In this approach we separate the rendering pipeline from the data acquisition pipeline through the use of a computational cluster where each node receives data from up to six microcameras and handles data requests from the rendering system. A memory manager is used to cache hundreds or thousands of frames based on image resolution while storing data to one or more solid state drives. Images requested from the rendering system are read from the cache or read from disk then resized to the appropriate scale before being sent. Using the computational cluster as a middle layer

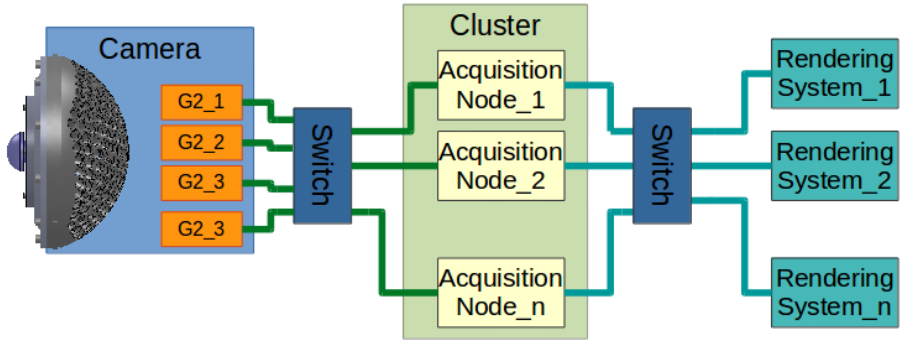

FIG. 3. Data routing architecture for the new AWARE camera

provides additional memory for caching, provides a common interface to multiple rendering systems, and provides scalable storage for gigapixel-scale data streams.

The rendering system uses an OpenGL framework similar to the one outlined in the previous paper to generate an interactive user interface. The raw bayer image data is demosaiced with GL shaders and mapped to a polygon mesh which is warped based on the sensor model as described in the section on the image processing pipeline. To increase the rendering update rate, a predictive algorithm is used to pre-fetch images from the computer cluster that are likely to be needed in upcoming frames. The aggressiveness of prediction is scaled based on available bandwidth and the computational resources of the cluster. In addition to the interface described in the previous paper, the current rendering application also provides a joystick interface for intuitive interaction with the data.

C. Camera Specifications and Testing

As we mentioned in section (I), one of the main objectives of this work was to reduce SWaP while maintaining optical imaging performance. The volume of the new system was approximately one third of the system described in [1] and less than half the weight (see again Figure 1 and the surrounding discussion). Identical optics (spherical objective lens) were used in both old and new AWARE camera systems although the newer system possessed a restricted field-of-view; obtained by reducing the number of micro-cameras to allow a more compact camera head package. This trade-off maintains the system resolution on the horizon (as compared to the older system) however would prohibit the detection or airborne targets that are beyond the 13° look-up angle. For maritime identification (our intended application) this trade-off (field-of-view for size, weight, and power) is appropriate.

The camera head is shown in Figure (1c) and has a 305 mm x 228 mm x 762 mm footprint and weighs 19 kilograms. Each camera required a 100 watt power supply and a water filled heat exchanger to dissipate heat generated by the 4 FPGAs inside each camera. The original camera used 2 kilowatts due to the increased number of image sensors (158 vs 30), however even correcting for the decreased number of cameras in this version of the system the power consumption is nearly an order of magnitude improvement.

All data communications between the camera head and the rendering computers was accomplished via single-mode SFP+ 10 Gigabits/second optical fiber transceivers. These signals were multiplexed using multi-wavelength transceivers to allow the entire 50 Gigabits/second of data to be relayed back to the computer cluster on 2 single-model fibers.

During field testing (see section III) the video from the camera was provided to an operator with a latency of under a second. A zoomed out view of the field-of-view is shown in Figure (4), approximately 53° × 13.6° with an instantaneous field-of-view of 25 micro-radians. Two AWARE cameras were used to speed up testing by allowing multiple trials to be run simultaneously using different regions of the full 180° FOV.

An example still frame from the test is shown in Figure 4. One of the camera sensors was malfunctioning that day which created the white circle in the lower-left corner. Each camera had 30 micro-cameras oriented in 3 rows of 11, 10, and 9 micro-cameras each. A zoomed in view from the top image is shown at the bottom of Figure (4) and shows the presence of an unknown watercraft. These images were both acquired using an external video recorder of the HDMI output from the rendering computer. The stitching model used was created during laboratory testing of the camera and hence there are minor stitching errors in the image. The flat field calibration is unable to exactly calibrate the color matching between sensors due to variances in the spectral response of each imaging sensor thus there are still minor color fluctuations between the micro-cameras.

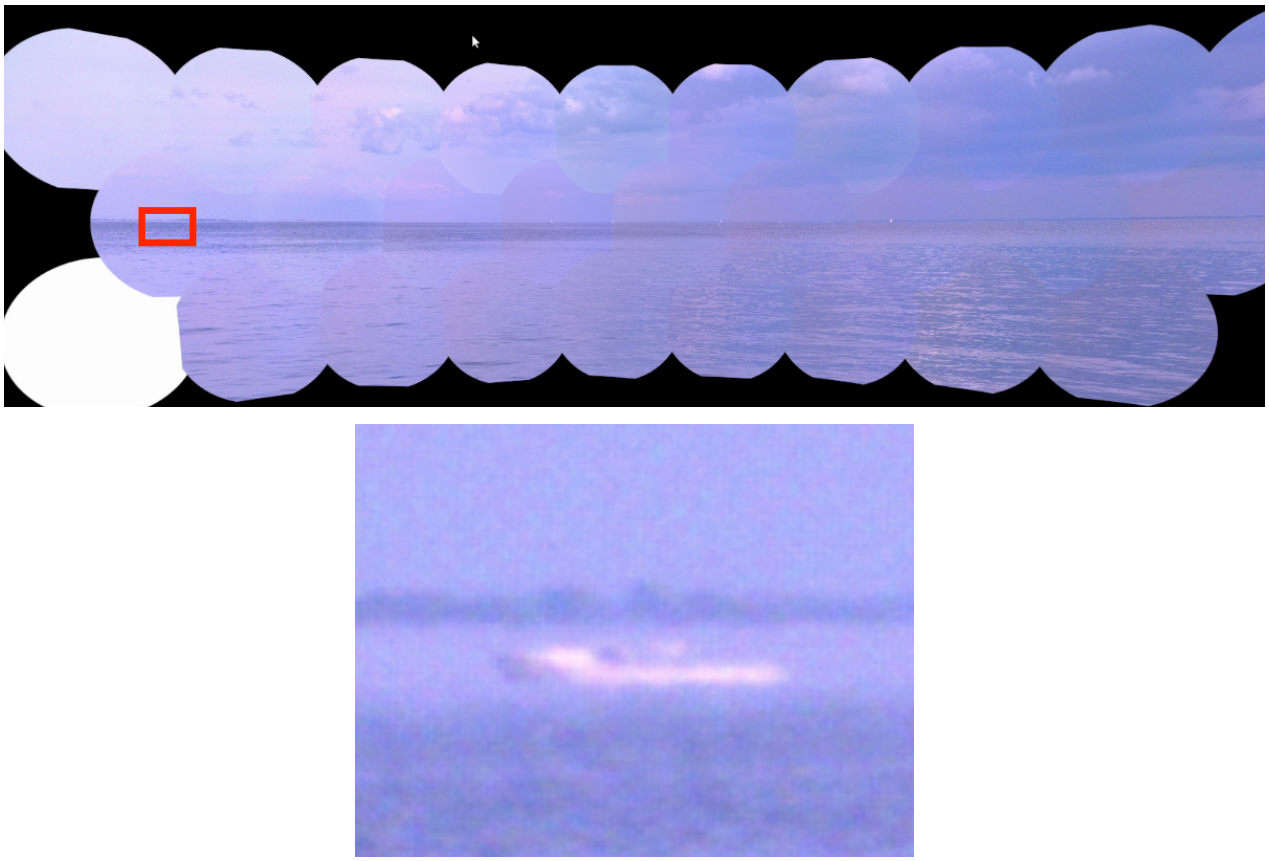

FIG. 4. Full panorama 53° by 13.6° image as displayed to the user with a box centered on a potential target (left) and a close-up of the target displayed. The camera is positioned at the end of a pier looking across the Chesapeake Bay toward Tighlman Island (barely visible on horizon).

III. RANGE PERFORMANCE

In this section we briefly review the range performance experiment and compare the new camera results to those obtained previously. Specifically, our focus is on assessing the range at which a typical observer can correctly identify a given target with 70% accuracy. This is a frequently-used criteria in assessing the relative performance of camera systems for maritime applications. In what follows we document the results obtained by from a maritime target identification experiment performed at the Naval Research Laboratory, Chesapeake Bay Detachment. The target set, camera location, and relevant ranges were retained from our prior work ([1]) in order to make the comparison as meaningful as possible. In fact, the experiments were performed over the same daylight hours and nearly the exact day of the year as the prior work.

The experiment consisted of placing one of three different target ships at a specific range and allowing a series of observers to attempt to identify the ship based on video imagery displayed on a computer monitor. The ships chosen were of a similar characteristic dimension in order to make the task more challenging. Specifically, the target ships (and their characteristic dimension) used in this study were: Duck boat (4m), Fishing boat (7m), and a Crab boat (10m). Each of these ships is shown in Fig. (5)

The computer monitors on which the imagery was displayed were housed in a large, climate controlled trailer. Once placed at range, the ships remained stationary and were always oriented broadside to the camera position so that the largest aspect was visible to the observer. Each observer was called separately into the trailer and given three minutes to search the image and record a response. Observers could respond with the ship(s) identified, report that no identification was possible, or report that no target was in the scene.

It is also worth noting that ambient maritime traffic created a number of false targets, or "clutter", during the testing. For any given trial, a number of other ships of similar size and type were in the FOV. While this created a challenging environment, it also effectively prevented the observers from simply guessing, or from using a "process of elimination" during trials in which multiple ships were in the scene. This is of particular importance in helping to

FIG. 5. Ships used in the maritime target identification experiment.

justify the assumption of "independent trials" used in the next section (see section III A). This same degree of clutter was present in our prior AWARE camera experiments.

A. Estimation Approach

The first step in any estimation procedure is to form a model for the observed data. To this end we make use of the same estimation procedure outlined in [1]. To briefly summarize, we assume the range performance model

$$p(r,s) = \frac{1}{1+\exp(a_{1s}r - a_{2s})},\ s = 1,2,3 \tag{2}$$

for target boat s at continuous range r. In what follows we use $s = 1$ (duck boat), $s = 2$ (fishing boat), and $s = 3$ (crab boat). The parameters a_{1s} and a_{2s} govern the rate at which identification probabilities decay from unity to zero and the range at which this transition occurs, respectively. The model (2) is simple, flexible, and accurately captures observer performance for a wide range of target detection experiments. Moreover, it allows us to use all available range data to estimate only two parameters per ship.

Given the model (2) for describing identification probability with range, and assuming all observer trials are independent, the model for the observer responses is given by the multinomial probability distribution

$$f_{\mathbf{K}_s}(\mathbf{k}_s(r_j)|\mathbf{a}_s) = \prod_{j=1}^{R} \frac{N_{js}!}{(1-k_s(r_j))!k_s(r_j)!}\left(1-\left(\frac{1}{1+\exp(a_{1s}r_j - a_{2s})}\right)\right)^{1-k_s(r_j)} \times \left(\frac{1}{1+\exp(a_{1s}r_j - a_{2s})}\right)^{k_s(r_j)} \tag{3}$$

where N_{js} are the number of trials conducted for ship class s at range $r_j,\ j = 1\cdots R$, and $k_s(r_j)$ are the number of those trials in which ship s was correctly identified. Given the data, $k_s(r_j)$, the goal is to estimate the parameters $a_{1s},\ a_{2s}$.

As in or prior work we take a Bayesian approach where we treat the parameters $a_{1s},\ a_{2s}$ as random variables $A_{1s},\ A_{2s}$. Our goal is to estimate the posterior probability distribution functions (PDFs) associated with each of these random variables. That is to say, given the k_s we estimate the posterior PDFs $f_{A_{1s}}(a_{1s}),\ f_{A_{2s}}(a_{2s})$ and then take the distribution mean as the final value for each of the parameters. We again use the Markov Chain Monte Carlo (MCMC) algorithm [3], which allows us to build a first order Markov chain for each parameter (and for each ship class) yielding M sample values $a_{1s}(j)$, $a_{2s}(j)$ $j = 1\cdots M$. For a properly formed chain (see [4] for details), the resulting $M-$vectors are comprised of samples from $f_{A_{1s}}(a_{1s}),\ f_{A_{2s}}(a_{2s})$. Our final parameter estimates are then simply $\hat{a}_{1s} = \frac{1}{M}\sum_{j=1}^{M} a_{1s}(j)$ and $\hat{a}_{2s} = \frac{1}{M}\sum_{j=1}^{M} a_{2s}(j)$ for each of the ship classes, s. These parameters then define the range performance via (2).

The chains are initialized with samples drawn from the uniform prior PDFs and are allowed some number of "burn-in" iterations B to converge to a stationary sequence of values. Values for subsequent iterations are then saved as samples from the posterior. Moreover, these samples can be used to estimate credible intervals (the Bayesian analogy of a confidence interval) by simply computing the upper and lower bounds on the central 95% of parameter values and the associated detection probabilities. Estimated range performance curves will be presented in the next section.

We note that this estimator of range performance is in contrast to the historical approach (see e.g., [5]) whereby probability of identification is estimated at each range separately and independently of data at other ranges. Specifically, the historical approach provides the maximum likelihood estimate (MLE) at each range via [4]

$$\hat{p}(r_j, s) = \frac{k_s(r_j)}{N_{js}}, \; j = 1 \cdots R, \tag{4}$$

where R is again the number of ranges over which data is acquired. While this approach was demonstrated conclusively to produce poor results in [6], the MLEs at each individual range will also be presented in the next section for comparison purposes.

B. Range Performance Results and Discussion

Based on the observer data, we used the MCMC algorithm to estimate the range performance parameters for each of the three ships. These results are displayed in the bottom row of Fig. (6) while the top row gives our prior results from the older AWARE camera system. The range performance curve associated with the maximum *a posteriori* estimate is given by the solid line while the 95% credible intervals are given by the dashed lines enveloping the estimated curve. For comparison purposes we have also plotted the MLEs, given by Eq. (4), associated with a given range. Finally, each curve also is annotated with the range at which 70% probability of identification was obtained. The 70% mark is frequently used in specifying requirements for EO/IR systems.

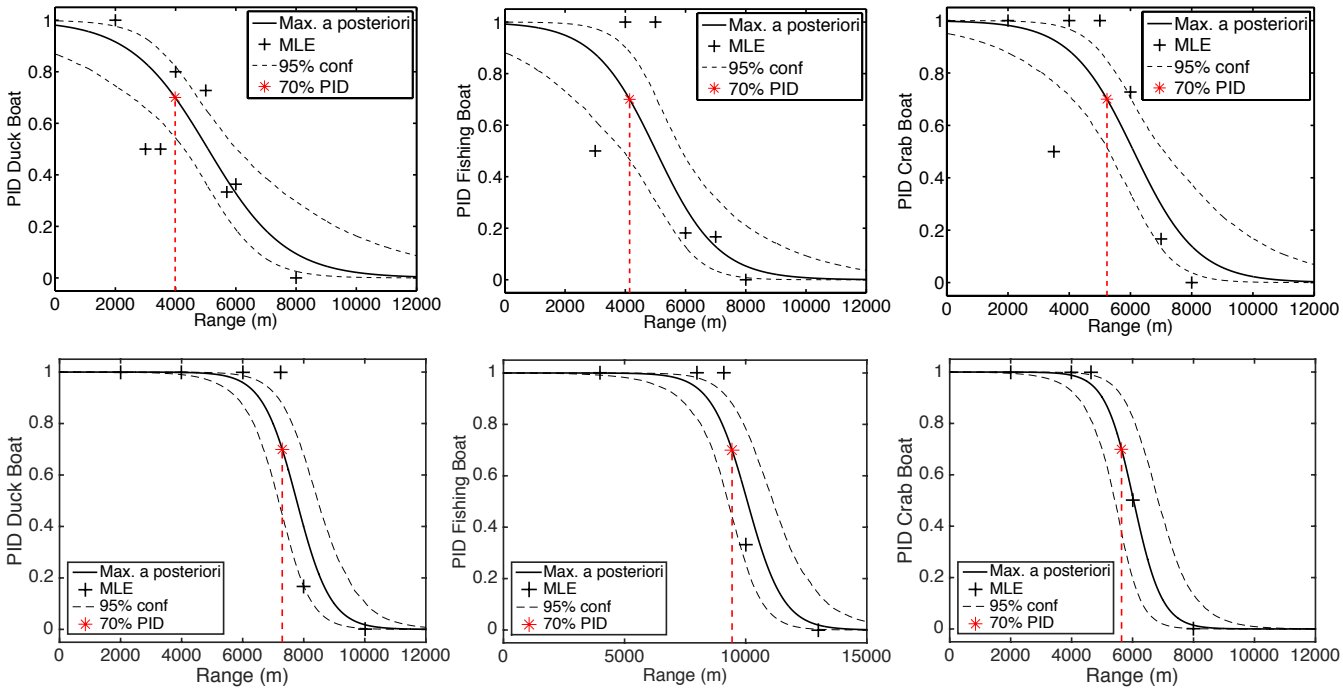

FIG. 6. Estimated range performance curves obtained using the MCMC algorithm. The top row shows the results of the prior AWARE camera (taken directly from [1] while the bottom row gives the results for the new system documented in this work. The maximum *a posteriori* curve is given by the solid line while the associated 95% credible interval is given by the dashed line. Also given are the maximum likelihood estimates at each range, denoted by crosses in the figure. The estimated 70% probability of identification range is highlighted with an asterisk.

For each of the classes of ship tested, performance was improved over our prior experiments. The improvement was most dramatic for both the duck boat and fishing boat. Both the duck boat and fishing boat improved by several kilometers their 70% identification points which, in this work, were found to be 7200m and 9500m respectively. This owes at least in part to the improved optics which significantly reduced the number of false classifications (i.e., crab

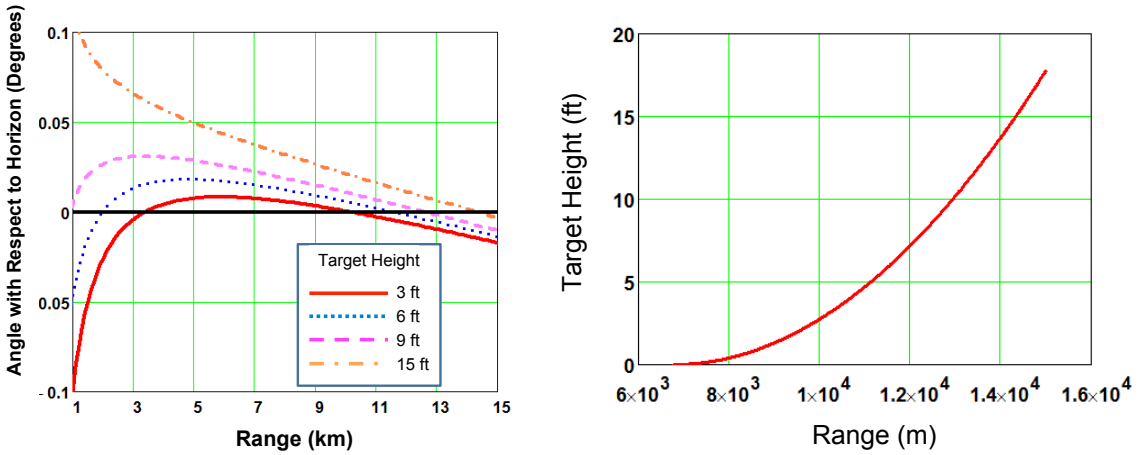

FIG. 7. (left) Angle between the camera line of sight and a point at various heights above the waterline. Once the angle becomes negative, a target of the depicted heights become completely obscured by the horizon. Displayed another way, the right hand plot gives the relationship between the obscured vertical dimension of the target and range.

boat being incorrectly identified as a duck boat). The crab boat also resulted in an improved range performance curve, although not as dramatic as for the other two ships.

In fact, the ranges at which the boats could be reliably identified increased nearly to the point at which they effectively disappear over the horizon. The camera was located at the end of a pier, roughly 12 feet above the waterline. Figure (7a) plots the angle between the camera line-of-sight to points at various heights above the water. Plotted another way Figure (7b) shows the obscured vertical dimension as a function of range. The duck boat is closest to the waterline, extending only a few feet above the surface, hence this boat is no longer visible at a distance of roughly 10km. This is consistent with the range performance curves of Fig. (6). Given the height of the superstructure on the fishing boat, this watercraft is the last to become fully obscured by the horizon, hence is reliably detected at the longer ranges.

It is also important to note that the confidence intervals for the estimated curves are a good deal more narrow than for the previous set of experiments. This stems from the significant drop in misclassifications. Whereas observers could detect the ships reliably with the previous AWARE camera, the non-uniformity in focus across the FOV was such that they often confused one ship for another, resulting in the larger variance in observer responses. This is in contrast to the current curves which drop suddenly once the critical detection range has been exceeded. The newer system produced significantly fewer misclassifications and only in a very narrow range of distances.

IV. CONCLUSIONS

A second generation of the AWARE visible imager was described and its performance characteristics reviewed. In addition to occupying a smaller footprint in terms of size and power, the system performed measurably better in a maritime range performance estimation task. We were able to quantitatively show a several kilometer improvement in identification ranges over the previous incarnation of the camera. We attribute most of the improvement to better focus in the optics across the field of view. While we cannot entirely rule out weather conditions as the reason for some of the improvement, all data were collected at the same times of day, (nearly) the exact same day of the year, and with no obvious difference in weather conditions from our previous data set.

ACKNOWLEDGMENTS

This project was supported by the DARPA MTO AWARE program under contract HR-0011-10-C-0073. We would also like to acknowledge the support of the Office of Naval Research “Program 38” for lending valuable resources to

this effort.

[1] D. L. Marks, P. R. Llull, Z. Phillips, J. G. Anderson, S. D. Feller, E. M. Vera, H. S. Son, S.-H. Youn, J. Kim, M. E. Gehm, D. J. Brady, J. M. Nichols, K. P. Judd, M. D. Duncan, J. R. Waterman, R. A. Stack, A. Johnson, R. Tennill, and C. C. Olson, "Characterization of the aware 10 two-gigapixel wide-field-of-view visible imager," Applied Optics **53**, C54–C63 (2014).

[2] H. Malvar, L. He, and R. Cutler, "High-quality linear interpolation for demosaicing of bayer-patterned color images," in "IEEE Conference on Acoustics, Speech, and Signal Processing (ICASSP)," , vol. 3 (2004), vol. 3, p. 85488.

[3] W. K. Hastings, "Monte carlo sampling methods using markov chains and their applications," Biometrika **57**, 97–109 (1970).

[4] J. M. Nichols, K. P. Judd, C. C. Olson, J. R. Waterman, and J. D. Nichols, "Estimating detection and identification probabilities in maritime target acquisition," Applied Optics **52**, 2531–2545 (2013).

[5] S. Moyer, J. G. Hixon, T. C. Edwards, and K. Krapels, "Probability of identification of small hand-held objects for electro-optic forward-looking infrared systems," Optical Engineering **46**, 063201 (2006).

[6] J. M. Nichols, J. Hines, and J. D. Nichols, "Selecting among competing models for electro-optic, infrared camera system range performance," Optical Engineering **52**, 113108 (2013).